Supplemental Methods

Radiosynthesis

Automated production of ^{18}F-THK5117 was performed on a Raytest® SynChrom R&D single reactor synthesizer. Solvent containers (SC) were loaded with reagents, and cartridges were assembled on the synthesizer. The manufacturing process was performed automatically using the Raytest® control software. No-carrier-added ^{18}F-fluoride was produced via ^{18}O(p, n)^{18}F reaction by proton irradiation of ^{18}O-enriched water and directly delivered to an ion exchange cartridge (Chromabond PS-HCO_3-, Macherey Nagel, Trap 1). The trapped ^{18}F-fluoride was eluted into the reactor using a mixture of Kryptofix®222 (12.5 mg), potassium carbonate (12.5 µL, 1 M), water (187.5 µL) and acetonitrile (800 µL) from SC 2. The solution was evaporated to dryness by azeotropic distillation, and the drying process was repeated after addition of acetonitrile (0.8 mL) from SC 3. The precursor (2 mg) in DMSO (0.7 mL) was transferred from SC 1 to the reactor, and the mixture was heated at 110°C for 10 min. HCl (0.2 mL, 2 M) from SC3 was then added, and the mixture stirred for 3 min. at 110°C. After quenching with AcOK (0.1 mL, 4 M) in H_2O (5 mL) from SC 4, the mixture was transferred to a SepPak tC18 Plus Short cartridge (Waters, Trap 2), which was then washed with H_2O (5 mL, SC wash). Radioactive products were eluted with EtOH/H_2O 1:1 (4 mL, SC Elute) and purified via semi-preparative HPLC (Inertsil ODS-4 C18 column, 250 x 10 mm, 5 µm; isocratic elution with 55% NaH_2PO_4 (20 mM) / 45% acetonitrile; flow: 5 ml/min; UV-detection: 360 nm). The HPLC purified product peak was collected in SC 11, diluted with H_2O (20 mL) and ascorbic acid (0.5 mL, 25%) from SC 8 and passed through a tC18 SepPak Plus Short cartridge (Waters, Trap 3). The radiolabelled product was eluted with anhydrous ethanol (1 mL) from SC 7 into the product vial, diluted with 0.9% saline (9 ml) from SC 9 and filtered through a sterile filter (Acrodisc®, 0.2 µm, PALL). The RCY was 16±2% (n=8) and RCP 99% with 75 min synthesis time. Purity was confirmed via analytical HPLC (Inertsil ODS-4 C18 column, 150 x 4.6 mm, 5 µm; isocratic elution with 50% NaH_2PO_4 (20 mM) / 50% acetonitrile; flow: 1.5 ml/min; UV-detection: 360 nm).

Animals

Animals were housed in a temperature- and humidity-controlled environment with a 12-hr light–dark cycle, with free access to food (Ssniff, Soest, Germany) and water.

Tau-P301S mice:

Transgenic Tau-P301S (P301S) mice express human P301S mutant 4R/0N Tau (Thy1-hTau.P301S) in CBA.C57BL/6 background (*1*). This model is characterized by tau hyperphosphorylation first and mainly in the brainstem, where tau filaments appear predominately as half-twisted ribbons. Larger AD-like paired helical filaments are observed less frequently. Behavioral defects manifest as early motor impairment at age 4 months and learning deficits from 2.5 months of age, leading to early death before 12 months of age. Four P301S mice aged 5.5 months and seven P301S mice aged 8-11 months were used for this study, compared to seven age-matched C57Bl/6 littermates serving as controls.

biGT mice:

Double transgenic biGT mice were developed by crossing Tau-P301L (P301L) homozygous transgenic mice with GSK3-β.S9A transgenic mice (*2*). The P301L mice express human 4R/2N-tau with the P301L mutation, under control of the murine THY1 promoter. Parental P301L mice show clinical symptoms from age 6-7 months, followed by intraneuronal tangles first and most markedly in the hindbrain (midbrain, brainstem, spinal cord), leading to death before age 12 months (*3*). biGT mice co-express Tau-P301L with constitutively active GSK3-β.S9A in the same neurons, leading to very severe tauopathy in cortex and hippocampus (*2*). These mice have an extended lifespan in comparison to P301L mice, ascribed to the less intense tauopathy in their hindbrain (*4*). The regional re-distribution is caused by GSK3-β dependent altered phosphorylation of Tau in the biGT mice. Tau depositions in biGT mice are highly fibrillar inclusions with the typical GSK3-β dependent phosphorylation signatures,

including S396/S404. The outcome is a very dramatic tauopathy in the forebrain of aged (14-18 months) biGT animals (*2*).

Eight biGT mice aged 12 months and eight biGT mice aged 21 months were analysed in this study. As age-matched FVB/N littermates were not available we additionally studied four C57Bl/6 and five Balb-C mice aged 12 months as well as four C57Bl/6 and five Balb-C mice aged 22 months. After exclusion of any age- or background-related differences in ^{18}F-THK5117 binding, the entire WT group (N=25) was pooled to allow increase of statistical power for VOI-based and statistical parametric mapping (SPM)-based analyses.

Tau-PET Data Acquisition and Analyses

Mice were anesthetized with isoflurane (1.5%, delivered at 3.5 l/min) and placed in the aperture of the Siemens Inveon DPET (*5*) as described previously (*6*).

P301S mice and seven age-matched C57Bl/6 controls were scanned in a full dynamic setting: upon injection to a tail vein of 16.1±2.4 MBq ^{18}F-THK5117 in 150 µl saline, a 90 min emission recording was initiated, followed by a 15 min transmission scan using a rotating ^{57}Co point source. Dynamic acquisitions consisted of 21 frames (3x1/6x2/9x5/3x10 min). Reconstruction was performed with 4 OSEM3D and 32 MAP3D iterations, and a zoom factor of 1.0, with scatter-, attenuation-, and decay-correction, resulting in a final voxel dimension of 0.78x0.78x0.80 mm.

Subsequently biGT mice and age-matched control mice were scanned with the single 30 min frame beginning 20 min after injection of 15.9±2.8 MBq ^{18}F-THK5117; all other parameters remained constant. Anaesthesia was maintained between injection and start of the µPET scan to exclude confounds from differing physiological state, and to ensure comparability between strains.

Following recovery from anaesthesia, mice were returned to their home cages, or were killed by cervical dislocation while still deeply anesthetized, prior to rapid brain removal.

Tau-PET Reader Independent Coregistration

To this end, SUV images were generated in this frame for all mice after the final manual MRI-atlas coregistration (TX_{rigid}). Attenuation and decay-corrected images of all TG and WT mice were averaged to generate a 20-50 min standard template. Non-linear brain normalization was performed with the PMOD fusion tool for all single frame SUV images coregistered to the MRI atlas to obtain transformation ($TX_{BrainNorm}$) for each mouse brain to the template. The manual (TX_{rigid}) and automatic ($TX_{BrainNorm}$) transformations were concatenated and applied to the native space µPET data to guarantee a minimum of interpolation. As the µPET templates had been initially aligned to the MRI mouse brain atlas, all final fused µPET images had the voxel dimensions of the MRI mouse brain atlas, i.e. 0.064 x 0.064 x 0.064 mm.

Immunohistochemistry

Following transcardial perfusion of the mice with phosphate buffered saline (PBS), brains were removed and fixed in 4% PFA in PBS over night at 4°C. 50 µm free-floating sections in the sagittal plane for P301S mice and in the coronal plane for biGT mice were cut on a vibratome (VT1000S, Leica Microsystems GmbH, Wetzlar, Germany). Two sections from each animal were analyzed, for P301S mice representative sections cut about 1.5 mm from the midline, for biGT mice sections -1.7 mm and -2.8 mm from bregma.

During all following steps, sections were kept on a shaker at room temperature. To permeabilize the tissue, the sections were incubated overnight in 2% Triton X-100 in PBS. Non-specific epitopes were blocked with Casein I-Block (Invitrogen) for 2 hours. AT8 antibody (Thermo Scientific) recognizing phospho-PHF-tau phosphorylated at Ser202 and Thr205 was

applied o/n, diluted 1:200 in Casein-I. Detection was performed by incubating the sections with secondary goat anti-rabbit antibody conjugated to Alexa Fluor 488 (1:500 in Casein-I; Life Technologies) for 4 hours. Sections were finally washed 3x15 min with casein-I before mounting on glass coverslips using fluorescence mounting medium (Dako, Glostrup, Denmark). 3D image stacks were acquired on an epi-fluorescence microscope (Axio Imager.M2 with ApoTome.2, Jena, Zeiss, Germany). Imaging of the whole slice was performed in tile scan mode, which allows automatic stitching of an array of fields of view with series of 10 µm z-stack projections.

The area and number of cells positive for AT8 were automatically counted using Imaris software (Imaris 7. 6.5; Bitplane, Zurich) in following regions of interest: for P301S mice the hindbrain part of brain stem (0.66±0.28 mm^3) and for biGT mice amygdalar nucleus, piriform, entorhinal and perirhinal cortical areas (0.33±0.08 mm^3) were assessed.

Methoxy-X04 staining was performed as described previously (*7*).

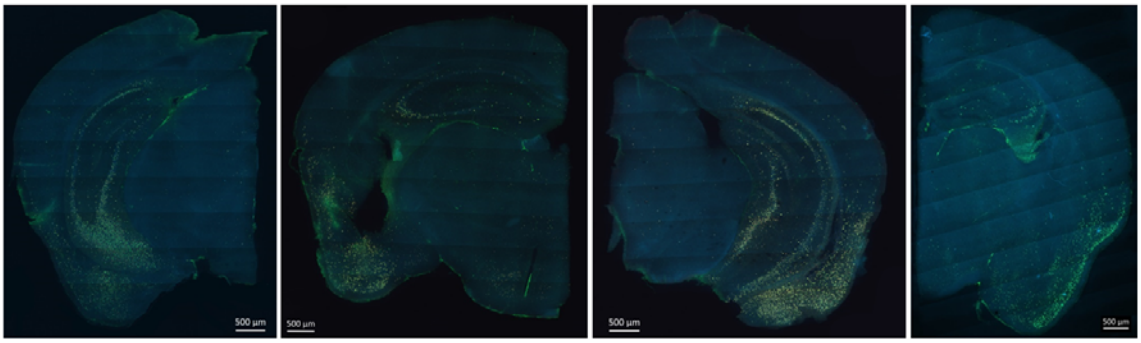

Supplemental Figure 1: Several AT8 stained coronal planes from biGT mice (all 21 months) are shown for illustrative purposes in order to give an impression on the regional heterogeneity.

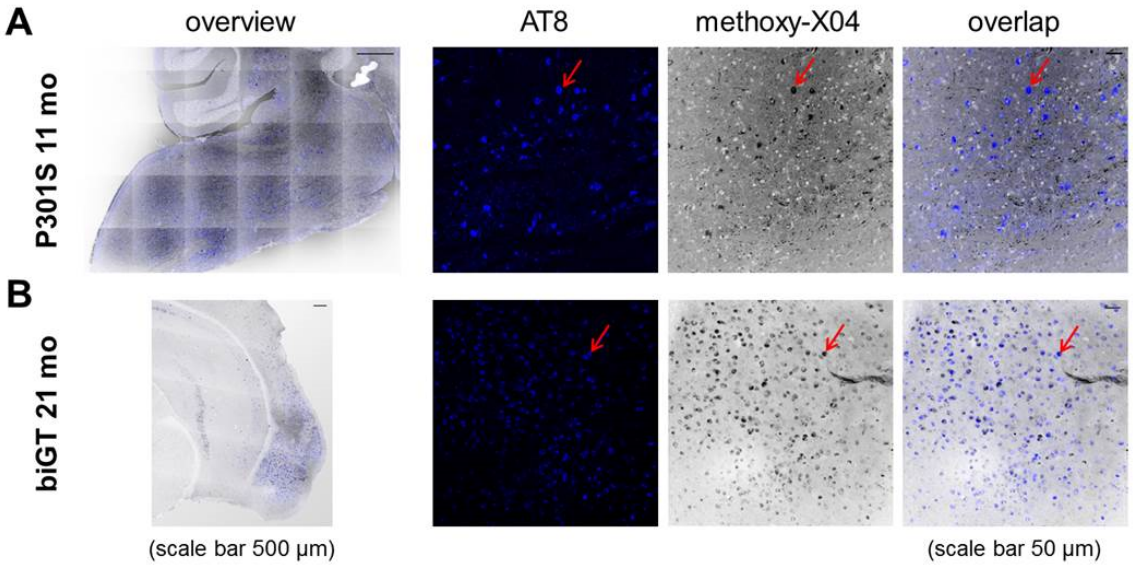

Supplemental Figure 2: Exemplary sagittal slice from a P301S mouse aged 11 months of the brainstem (A) and a sagittal slice from a biGT mouse aged 21 months of entorhinal and post-piriform cortices (B). In the zoomed panels from left to right: AT8 staining for hyperphosphorylated tau, methoxy-X04 staining for β-sheet structures, as well as the fusion indicating a high overlap. Red arrows indicate tau deposition which is depicted by both AT8 and methoxy-X04 staining.

Ex Vivo and *In Vitro* Autoradiography

Brains were resected and immediately frozen by immersion in isopentane at –40 ºC, mounted in a cryostat (Leica CM 1510-1, Leica Microsystems, Nussloch, Germany), and, after thermal equilibration at – 20 ºC for 30 min prior, were cut into 20 µm thick sections in the sagittal plane. Selected sections were mounted on glass slides and placed on Fujifilm BAS cassette2 2025 imaging plates. The plates were exposed for six hours and then scanned at 25 µm resolution with the Raytest equipment (CR-35-BIO, Dürr Medical, Germany). Resulting images were analyzed with dedicated software (AIDA image analysis, V4.50, Raytest GmbH, Straubenhardt, Germany). 50-µm thick coronal brain sections from biGT mice neighbouring previously immunohistochemically analysed sections were used for autoradiography *in vitro*.

Slide-mounted brain sections were first pre-incubated with binding buffer (Tris-HCl 50 mM, pH 7.4) and then dried, prior to incubation in 2 nM ^{18}F-THK5117 for 60 minutes at room temperature. Blocking studies were made with the addition of 10 μM THK5117 to the incubation mixture in order to prove saturable binding. Slides were then washed by immersion in ice-cold binding buffer (3 times, 30 seconds each), rapidly dried under an air stream, and then placed on imaging screens for six hours, prior to digitization and analysis as described above. 20 μm slices originating from P301S and C57Bl/6 *ex vivo* autoradiography were as well co-analysed with *in vitro* technique (without blocking) for visual purposes.

Supplemental Limitations

Hot Spot. In 6/18 (33%) of our mice with C57Bl/6 background (TG and WT) we saw a hot-spot of ^{18}F-THK5117 accumulation lying between the frontal pole and the olfactory bulb, the intensity of which increased with scanning time. This hot spot was clearly confirmed by autoradiography *ex vivo* (see Supplemental Fig. 3), but was absent in corresponding slices examined by autoradiography *in vitro*, and was also lacking to immunohistochemical examination. We suppose that this focal radioactivity accumulation may be related to sinusoidal drainage or distortion of the adjacent mucosa. In the absence of a definite anatomical/physiological explanation, the intermittent hot-spot presents a limiting factor for quantitation of ^{18}F-THK5117 binding in the mouse frontal cortex.

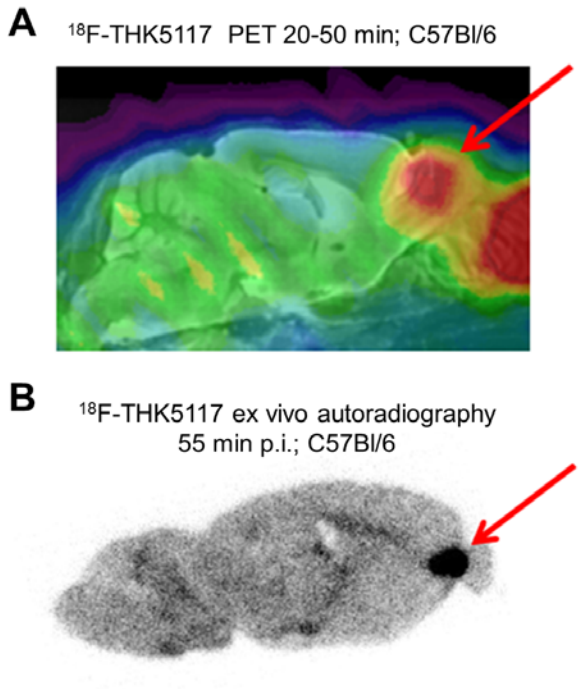

Supplemental Figure 3: Illustration of the unexpected frontal hot spot in µPET (A) and corresponding *ex vivo* autoradiography (B).

Translational Aspect. Tau depositions in both of the transgenic models originate from FTLD mutations with and without additional GSK3-β overexpression to induce a more intense and AD-like tau pathology. While our study clearly proves the principle of *in vivo* imaging of tau pathology, the model differences must be considered for translational validity to AD. In general, rodent models best emulating the human AD tau pathology present an advantage for translation, in presenting the best possible congruence between rodent and human molecular imaging.

Background. Age-matched FVB/N and/or single transgenic GSK3-β.S9A controls as the appropriate background for biGT mice were not available. Thus we cannot fully exclude a bias resulting from the substitution of age-matched C57Bl/6 and Balb-C mice. Nonetheless we did not observe any age- or background-related differences in cerebral ^{18}F-THK5117 binding of C57Bl/6 and Balb-C mice. Furthermore, correlation analyses of µPET estimates and

immunohistochemistry in the transgenic animals confirmed the validity of biGT μPET results, irrespective from findings in WT animals.

Structural information. Our present instrumentation does not afford hybrid imaging, but we concur that small animal PET-MRI (or PET-CT) hybrid imaging could further improve quantitation of preclinical Tau imaging, especially with regard to effects of atrophy. For the present, stand-alone PET studies must suffice, since the hybrid PET-MRI systems are still not widely available. Based on our experience, we feel that automatized non-linear brain normalization can partially accommodate inter-animal variability with regard both to variance between the strains and between individual mice. As the PET template used for this spatial normalization was obtained as a composite of all individual MRI-atlas-fused images, we can assume a high degree of agreement between spatially normalized PET images with the MRI mouse brain atlas for both strains.

Supplemental References

1. Allen B, Ingram E, Takao M, et al. Abundant tau filaments and nonapoptotic neurodegeneration in transgenic mice expressing human P301S tau protein. *J Neurosci.* 2002;22:9340-9351.

2. Terwel D, Muyllaert D, Dewachter I, et al. Amyloid activates GSK-3beta to aggravate neuronal tauopathy in bigenic mice. *Am J Pathol.* 2008;172:786-798.

3. Terwel D, Lasrado R, Snauwaert J, et al. Changed conformation of mutant Tau-P301L underlies the moribund tauopathy, absent in progressive, nonlethal axonopathy of Tau-4R/2N transgenic mice. *J Biol Chem.* 2005;280:3963-3973.

4. Crespo-Biel N, Theunis C, Borghgraef P, et al. Phosphorylation of protein Tau by GSK3beta prolongs survival of bigenic Tau.P301LxGSK3beta mice by delaying brainstem tauopathy. *Neurobiol Dis.* 2014;67:119-132.

5. Visser EP, Disselhorst JA, Brom M, et al. Spatial resolution and sensitivity of the Inveon small-animal PET scanner. *J Nucl Med.* 2009;50:139-147.

6. Rominger A, Mille E, Zhang S, et al. Validation of the octamouse for simultaneous 18F-fallypride small-animal PET recordings from 8 mice. *J Nucl Med.* 2010;51:1576-1583.

7. Rominger A, Brendel M, Burgold S, et al. Longitudinal assessment of cerebral beta-amyloid deposition in mice overexpressing Swedish mutant beta-amyloid precursor protein using 18F-florbetaben PET. *J Nucl Med.* 2013;54:1127-1134.